DMD Fast Forward. Published on June 21, 2006 as doi:10.1124/dmd.106.010934

Using A Tritiated Compound to Elucidate Its Preclinical Metabolic and Excretory Pathways *In Vivo*: Exploring Tritium Exchange Risk

Christopher L. Shaffer, Mithat Gunduz[1], Bruce A. Thornburgh and Gwendolyn D. Fate

Department of Pharmacokinetics, Pharmacodynamics and Metabolism, Pfizer Global Research and Development, Pfizer Inc., Groton, Connecticut (C.L.S., M.G.) and Kalamazoo, Michigan (B.A.T., G.D.F.)

DMD Fast Forward. Published on June 21, 2006 as DOI: 10.1124/dmd.106.010934
This article has not been copyedited and formatted. The final version may differ from this version.

Running Title: *In Vivo* Metabolite Identification Using Tritium

Address correspondence to:

Dr. Christopher L. Shaffer
Pharmacokinetics, Dynamics and Metabolism
Pfizer Global Research and Development
Groton/New London Laboratories
Pfizer Inc.
Eastern Point Road, MS 8220–4186
Groton, CT 06340
Tel. 860.441.3377
Fax 860.686.6532
Email: Christopher.L.Shaffer@pfizer.com

Text pages: 32
Tables: 4
Figures: 7
References: 30
Words in Abstract: 249
Words in Introduction: 750
Words in Discussion: 1,489

Abbreviations: 1, *N*-(3*R*)-1-azabicyclo[2.2.2]oct-3-ylfuro[2,3-c]pyridine-5-carboxamide (2*E*)-2-butanedioate; [^{3}H]**1a**, 3-tritio-*N*-(3*R*)-1-azabicyclo[2.2.2]oct-3-ylfuro[2,3-c]pyridine-5-carboxamide hydrochloride; [^{3}H]**1b**, 7-tritio-*N*-(3*R*)-1-azabicyclo[2.2.2]oct-3-ylfuro[2,3-c]pyridine-5-carboxamide ditrifluoroacetate; **2**, *N*-(3*R*)-1-azabicyclo[2.2.2]oct-3-ylcarbamoyl-5-hydroxypyridin-4-yl-acetic acid; **3**, *N*-(3*R*)-1-azabicyclo[2.2.2]oct-3-ylcarbamoyl-5-hydroxypyridine-4-carboxylic acid; **4**, *N*-(3*R*)-1-azabicyclo[2.2.2]oct-3-ylfuro[2,3-c]pyridine-5-carboxamide-1-*N*-oxide; PK, pharmacokinetic(s); AUC, area under the plasma concentration-time curve; LSC, liquid scintillation counting; k_{el}, elimination rate constant; C_{max}, maximal plasma concentration; LLOQ, lower limit of quantification; LC-MS/MS, liquid chromatography-tandem mass spectrometry; rcf, relative centrifugal force; HPLC, high-performance liquid chromatography; LC t_R, liquid chromatography retention time; CID, collision-induced dissociation.

DMD Fast Forward. Published on June 21, 2006 as DOI: 10.1124/dmd.106.010934
This article has not been copyedited and formatted. The final version may differ from this version.

Abstract

The metabolism and excretion of *N*-(3*R*)-1-azabicyclo[2.2.2]oct-3-ylfuro[2,3-c]pyridine-5-carboxamide (**1**), an agonist of the α_7 nicotinic acetylcholinergic receptor, were determined in both Sprague-Dawley rats and beagle dogs using [^{3}H]**1**. Initially, 3-tritio-furanopyridine **1** ([^{3}H]**1a**) was evaluated in pilot mass balance studies by determining total radioactivity recovery and pharmacokinetics in lyophilized excreta and non-lyophilized plasma, respectively. Lower mass balance and much greater circulatory radioactivity exposures were observed in rats than in dogs, with urinary tritiated water (HTO) only detected in rats. The 133 h half-life in rats, possibly due to very slowly eliminated metabolites, was more likely attributable to HTO formed from [^{3}H]**1a** due to site-specific chemical and/or metabolic ^{3}H-instability, which was confirmed by urinary HTO. Contrastingly, dog data supported ^{3}H-stability within [^{3}H]**1a**. Conflicting cross-species data with [^{3}H]**1a** suggested species-specific metabolic fates for **1** requiring a ^{3}H-form of **1** resistant to ^{3}H-loss in rats. Accordingly, tritiation of **1** at its furanopyridine C_7, a site predicted to be both chemically and metabolically stable, yielded [^{3}H]**1b**, which allowed in both species the determination of all excretory pathways, total radioactivity pharmacokinetics, and major excretory and circulatory metabolites with complete radioactivity recovery without HTO generation. Definitive metabolite elucidation for **1** using [^{3}H]**1b** confirmed the suspected species-dependent metabolic susceptibility for ^{3}H-loss from [^{3}H]**1a** in rats, but not dogs, as the majority of rat metabolites resulted from furanopyridine biotransformation. The described studies explore the evaluation of tritium exchange risk from a mechanistic biotransformation perspective and highlight the need

for careful deliberation when considering and designing ^{3}H-compounds for radiolabeled metabolism studies.

DMD Fast Forward. Published on June 21, 2006 as DOI: 10.1124/dmd.106.010934
This article has not been copyedited and formatted. The final version may differ from this version.

Introduction

Radioisotope use in biopharmaceutical research has been invaluable in elucidating definitively test compound excretory and metabolic pathways in animals (Dalvie, 2000). The most common radionuclide used for these studies is ^{14}C due to its synthetic versatility, safety relative to other radioisotopes and favorable nuclear properties dictating optimal half-life and specific activity (McCarthy, 2000). However, in certain instances, ^{3}H has been used instead of (or in addition to) ^{14}C to attain *in vitro* (Guroff et al., 1967; Kler et al., 1992; Linnet, 2004) and *in vivo* (Prakash et al., 1997; Ehlhardt et al., 1998; Koller-Lucae et al., 1999; Rosenborg et al., 1999; Gray et al., 2001) biotransformation data. Due to the general synthetic ease, low cost and rapid turnaround of ^{3}H-incorporation (Saljoughian and Williams, 2000), such high specific activity compounds are desirable when radiolabeled material is needed quickly to answer particular metabolism-related questions during drug discovery or development.

Although a compound's ^{14}C atom may become separated from the substructure retained by the majority of metabolites due to its incorporation at a metabolically labile site (Chasseaud et al., 1974; Hawkins et al., 1977; Larsson and Lund, 1981), there is no concern of its passive chemical exchange leading to non-radiolabeled compound and/or metabolites. Conversely, due to the intrinsic properties of the hydrogen atom, ^{3}H-exchange within a molecule may occur readily in aqueous physiological environments of varying pH by chemical (e.g. α-H exchange during keto-enol tautomerization) or metabolic means (Lewis et al., 1988). In either case, ^{3}H-exchange ultimately affords tritiated water (HTO), the molecular reporter of ^{3}H-loss, resulting in both the absence of radiotracer capabilities from the test compound and/or its metabolites and ambiguous

DMD Fast Forward. Published on June 21, 2006 as DOI: 10.1124/dmd.106.010934
This article has not been copyedited and formatted. The final version may differ from this version.

biotransformation data. Hence, the predominant risk associated with using ^{3}H-labeled compounds in biological systems is the potential chemical and metabolic instability of the ^{3}H atom itself at its specific site within the test molecule. For instance, when profiling *in vitro* or *in vivo* samples containing ^{3}H-metabolites requiring identification, formed HTO might be detected radiochromatographically within the solvent front potentially resulting in its erroneous identification as a highly polar (and possibly significant) metabolite. Similarly, ambiguity might arise when calculating ^{3}H-recovery from biofluids undergoing organic extraction; low organic phase ^{3}H-levels may be ascribed to highly polar metabolites, HTO or both. For total radioactivity PK analyses, ^{3}H-exchange causes similar data interpretation complexities due to tritium's three-component exponential function biological half-life, ranging from 10–300 days in humans (Robertson, 1973). If ^{3}H-exchange occurs, the total radioactivity AUC is useless since its terminal phase can be attributable to HTO and not necessarily drug-related material (Kim et al., 2004). Therefore, to use ^{3}H-compounds effectively for drug metabolism studies, one must not only strategically select the theoretically most chemically- and metabolically-stable molecular site for ^{3}H-incorporation, but also seek empirical confirmation by quantifying HTO within all samples via lyophilization to determine the true inertness of the ^{3}H atom.

With these issues in mind, **1**, an agonist of the α_7 nicotinic acetylcholinergic receptor (Wishka et al., 2006), was selectively monotritiated for radiolabeled mass balance studies in Sprague-Dawley rats and beagle dogs. Initially, [^{3}H]**1a** (Figure 1) was generated due to synthetic ease, and its suitability in both species was evaluated in pilot studies by determining ^{3}H-recovery in lyophilized urine and feces, and ^{3}H AUC using non-lyophilized plasma. Only 80% mass balance was achieved in rats with urinary HTO

accounting for 4% of recovered dose, while 95% mass balance was attained in dogs with no detection of HTO. Furthermore, [^{3}H]**1a** afforded total radioactivity half-lives of 133 and 5 h in rats and dogs, respectively (Figure 2). The incredibly long half-life in rats was indicative of very slowly eliminated metabolite(s) and/or HTO formed from drug-derived material attributable to site-specific chemical and/or metabolic ^{3}H-instability (Figure 3); the latter was confirmed by urinary HTO. Conversely, dog data suggested ^{3}H-stability within [^{3}H]**1a** due to no metabolism of **1** (and the chemical stability of ^{3}H within **1**) and/or the conversion of **1** to ^{3}H-retaining metabolites (Figure 3). Conflicting species-dependent ^{3}H-recovery and PK data implicated different metabolic fates for **1** in rats and dogs, and demonstrated the need for a ^{3}H-form of **1** impervious to ^{3}H-loss in rats. Accordingly, ^{3}H-incorporation at a site predicted to be both chemically and metabolically stable yielded [^{3}H]**1b** (Figure 1). Using [^{3}H]**1b** in rats and dogs, all excretory pathways, total radioactivity PK, and major excretory and circulatory metabolites were identified definitively with complete radioactivity recovery in both species without HTO generation. Studies characterizing and rationalizing the metabolites of **1** are described herein that ultimately explain species-dependent ^{3}H-loss with [^{3}H]**1a**, but not [^{3}H]**1b**.

DMD Fast Forward. Published on June 21, 2006 as DOI: 10.1124/dmd.106.010934
This article has not been copyedited and formatted. The final version may differ from this version.

Materials and Methods

Chemicals and Reagents. Compounds **1** (Wishka et al., 2006), **2**, **3** and **4** were made by the Synthesis Group at Pfizer Global Research and Development (PGRD, Kalamazoo, MI); [^{3}H]**1a**•2HCl (10 Ci/mmol, 99.9% radiochemical purity) and [^{3}H]**1b**•2TFA (17 Ci/mmol, 100% radiochemical purity) were synthesized (Maxwell et al., 2006) by the Radiochemical Synthesis Group at PGRD (Kalamazoo, MI). The chemical purity of all synthetic compounds was >99%. Chemicals and solvents of reagent or HPLC grade were supplied by Aldrich Fine Chemical Co. (Milwaukee, WI), Cambridge Isotope Laboratories, Inc. (Cambridge, MA), Fisher Scientific (Pittsburgh, PA) and the J. T. Baker Chemical Co. (Phillipsburg, NJ). All excreta and plasma were collected gravimetrically and stored at –20 °C until analysis.

Characterization of Synthetic Standards 1, 2, 3 and 4. The syntheses and full characterization of **1** (Wishka et al., 2006), and [^{3}H]**1a** and [^{3}H]**1b** (Maxwell et al., 2006) are reported elsewhere. For the characterization of metabolite authentic standards **2**, **3** and **4**, an OXFORD AS400 spectrometer (OXFORD Instruments, Eynsham Witney, Oxon, UK) was used to obtain ^{1}H NMR spectra at 400 MHz and ^{1}H-decoupled ^{13}C NMR spectra at 100.5 MHz. Proton chemical shifts are reported in ppm (δ) relative to tetramethylsilane as inferred from shifts of residual protons in employed deuterated solvents (i.e. 4.80 ppm for D_2O, 2.50 ppm for d_6-DMSO and 3.31 ppm for CD_3OD); ^{13}C chemical shifts are in ppm relative to internal solvent carbons (i.e. 39.51 ppm for d_6-DMSO and 49.15 ppm for CD_3OD).

*Compound **2***. ^{1}H NMR (400 MHz, D_2O) δ 1.96 (m, 1H), 2.09 (m, 2H), 2.24 (m, 1H), 2.38 (m, 1H), 3.26–3.43 (m, 5H), 3.60 (s, 2H), 3.82 (t, J = 9.2 Hz, 1H), 4.44 (m,

DMD Fast Forward. Published on June 21, 2006 as DOI: 10.1124/dmd.106.010934
This article has not been copyedited and formatted. The final version may differ from this version.

1H), 7.78 (s, 1H), 8.12 (s, 1H); ^{13}C NMR (100.5 MHz, D_2O) δ 16.96, 21.35, 24.09, 39.35, 44.91, 46.19, 46.63, 52.25, 125.51, 133.98, 137.08, 140.57, 155.26, 167.52, 178.69; ESI: $[M+H]^+$ = 306; Elemental analysis calcd for $C_{15}H_{19}N_3O_4$ C: 58.35, H: 6.37, N: 13.53; found, C: 58.49, H: 6.38, N: 13.57.

*Compound **3**.* ^{1}H NMR (400 MHz, d_6-DMSO) δ 1.70 (m, 1H), 1.90 (m, 2H), 2.04 (m, 1H), 2.16 (m, 1H), 3.14–3.37 (m, 5H), 3.62 (t, *J* = 11.4 Hz, 1H), 4.33 (m, 1H), 8.08 (s, 1H), 8.18 (s, 1H), 8.72 (s, 1H), 8.74 (s, 1H), 9.41 (s, 1H); ^{13}C NMR (100.5 MHz, d_6-DMSO) δ 17.19, 21.51, 24.56, 43.88, 45.22, 45.60, 50.73, 122.18, 124.62, 136.79, 139.26, 163.61, 164.77, 169.10; ESI: $[M+H]^+$ = 292; Elemental analysis calcd for $C_{14}H_{17}N_3O_4$ C: 57.53, H: 5.90, N: 14.38; found, C: 57.26, H: 5.88, N: 14.26.

*Compound **4**.* ^{1}H NMR (400 MHz, CD_3OD) δ 2.06 (m, 1H), 2.19 (m, 2H), 2.26 (m, 1H), 2.35 (m, 1H), 3.38–3.51 (m, 5H), 3.81 (t, *J* = 11.6 Hz, 1H), 7.11 (d, *J* = 2.1 Hz, 1H), 8.11 (d, *J* = 1.7 Hz, 1H), 8.43 (s, 1H), 8.91 (s, 1H); ^{13}C NMR (100.5 MHz, CD_3OD) δ 22.26, 25.35, 26.66, 63.12, 63.48, 68.82, 72.32, 108.15, 117.26, 133.73, 136.75, 144.51, 151.69, 155.23, 167.30; ESI: $[M+H]^+$ = 288; Elemental analysis calcd for $C_{15}H_{17}N_3O_3$ C: 58.71, H: 6.31, N: 13.66; found, C: 58.76, H: 6.39, N: 13.70.

***In Vivo* Studies with [^{3}H]1a and [^{3}H]1b.** The in-life portions of both rat and dog studies using [^{3}H]**1a** were conducted at PGRD (Kalamazoo, MI), while those for rats and dogs with [^{3}H]**1b** were performed at Covance, Inc. (Madison, WI) and Charles River Laboratories International, Inc. (Worcester, MA), respectively. All animal studies were conducted in accordance with the Guide for the Care and Use of Laboratory Animals, and all study animals were fasted overnight prior to compound administration and for 4 h post-dose. Individual animal doses were calculated based on respective pre-treatment

DMD Fast Forward. Published on June 21, 2006 as DOI: 10.1124/dmd.106.010934
This article has not been copyedited and formatted. The final version may differ from this version.

body weights and a dose volume appropriate for the specific species. The actual amount of dose solution administered to each animal was determined by weighing the loaded dosing syringe before and after it was dispensed.

*[^{3}H]**1a** in SD Rats.* A single dose (8 mg/kg, 400 μCi) of [^{3}H]**1a** in citrate buffer (50 mM, pH 5) was administered via oral gavage to intact male rats. The study included two groups of rats: Group 1 (2 males): Urine, feces and cage rinse were collected from animals pre-dose and in 24 h intervals over 4 days post-dose; and, Group 2 (1/time point): Blood samples from animals euthanized pre-dose and at 0.5, 2 and 8 h post-dose were collected by exsanguination following cardiac puncture into tubes containing Na_2EDTA and processed to obtain plasma.

*[^{3}H]**1a** in Beagle Dogs.* A single dose (15 mg/kg, 640 μCi) of [^{3}H]**1a** in citrate buffer (50 mM, pH 5) was administered orally to a single intact male dog. From this one dog excreta and cage debris/rinse were collected pre-dose and in 24 h intervals over 2 days, while blood samples (ca. 6 mL) were collected into heparinized tubes via venipuncture of a cephalic or jugular vein pre-dose and at 0.5, 1, 2, 4, 8 and 24 h post-dose, and processed to obtain plasma.

*[^{3}H]**1b** in SD Rats.* A single dose (5 mg/kg, 25 μCi) of [^{3}H]**1b** in citrate buffer (50 mM, pH 5) was administered via oral gavage to each intact rat. The study included two groups of rats: Group 1 (4/sex): From intact animals, urine was collected pre-dose and from 0–12 and 12–24 h during Day 1, and in 24 h intervals from 24–168 h post-dose. From the same animals, feces and cage rinse were collected pre-dose and in 24 h intervals from 0–168 h post-dose; and, Group 2 (1/sex/time point): Blood samples from intact

animals euthanized pre-dose and at 0.5, 1, 2, 4, 8 and 24 h post-dose were collected by cardiac puncture into tubes containing Na_2EDTA and processed to obtain plasma.

*[^{3}H]**1b** in Beagle Dogs.* A single dose (10 mg/kg, 480 μCi) of [^{3}H]**1b** in citrate buffer (50 mM, pH 5) was administered orally to intact dogs (2/sex) from which excreta and cage debris/rinse were collected as described for [^{3}H]**1b** in rats. Blood samples (ca. 6 mL) were collected into heparinized tubes via venipuncture of a cephalic or jugular vein pre-dose and at 0.25, 0.5, 1, 2, 3, 4, 6, 8, 12 and 24 h post-dose, and processed to obtain plasma. Control plasma was harvested from blood collected from untreated dogs.

Determination of Radioactivity Within Urine and Plasma from Animals Receiving [^{3}H]1a. Due to the exploratory nature of the [^{3}H]**1a** studies, only urine was subjected to lyophilization to determine its HTO concentration. Therefore, duplicate non-lyophilized gravimetric aliquots of urine (0.5 g) and plasma (0.1 g) from each time point were mixed with Ultima Gold™ (PerkinElmer Life and Analytical Sciences, Inc., Wellesley, MA) liquid scintillation cocktail (15 mL) and counted for 2 min by a Packard Tri-Carb 1900CA or 2300TR liquid scintillation counter (Packard BioScience, Co., Meriden, CT). In parallel, duplicate gravimetric aliquots (2 g) of urine from each time point were frozen, lyophilized using a FreeZone 4.5 Benchtop Freeze Dry System (Labconco Corp., Kansas City, MO), reconstituted in Milli-Q H_2O (0.2 g) and liquid scintillation cocktail (15 mL), and analyzed for total radioactivity by LSC for 2 min. The difference in total radioactivity within each urine sample before and after lyophilization was attributed to HTO. Scintillation counter data were automatically corrected for counting efficiency using an external standardization technique and an instrument-stored quench curve generated from a series of sealed quench standards.

Determination of Radioactivity Within Urine and Plasma from Animals Receiving [^{3}H]1b. The following procedure was undertaken to quantify both total radioactivity and HTO within each urine and plasma sample: Triplicate gravimetric aliquots (0.2–0.5 g for urine, 0.05 g for plasma) from each time point were mixed with TruCount scintillation cocktail (15 mL) and counted for 2 min by a Model LS 6000 or LS 6500 liquid scintillation counter (Beckman Coulter, Inc., Fullerton, CA). In parallel, triplicate gravimetric aliquots of similar mass from each time point were frozen, lyophilized, reconstituted and analyzed for total radioactivity as previously described. The difference in total radioactivity within each sample without and with lyophilization was ascribed to HTO. Scintillation counter data were automatically corrected for counting efficiency as described for [^{3}H]**1a**.

Determination of Radioactivity Within Feces and Cage Debris/Rinse from Animals Receiving [^{3}H]1a or [^{3}H]1b. Fecal samples were homogenized with Milli-Q H_2O (20% w/w, feces/H_2O) using a probe-type or Stomacher homogenizer. Cage debris/rinse samples (collected in 50% reagent alcohol in H_2O) were homogenized directly with a probe-type homogenizer. Triplicate gravimetric aliquots (0.4–0.7 g for either homogenate) were transferred into tared cones and pads, weighed, dried for a minimum of 24 h at ambient temperature, and combusted prior to radioanalysis. Sample combustion was performed using a Packard Instruments Model A0387 sample oxidizer (Packard BioScience, Co., Meriden, CT). Combustion efficiency using a ^{3}H-standard was determined daily prior to the combustion of study samples, and the measured radioactivity content in feces and cage debris/rinse was adjusted using daily combustion efficiency values. Liberated HTO was trapped in Monophase-S® (Perkin Elmer Life and

Analytical Sciences, Boston, MA), mixed in Perma-Fluor-E scintillation fluid (Packard BioScience, Co., Meriden, CT) and quantified in a Model LS 6000 or LS 6500 liquid scintillation counter (Beckman Coulter, Inc., Fullerton, CA) for 10 min. All combustion-related scintillation counter data were corrected for counting efficiency as explained previously.

Pharmacokinetic Calculations. PK parameters were calculated for each gender (rats) or animal (dogs) by non-compartmental analyses using WinNonlin Version 3.2 (Pharsight Corp., Mountain View, CA). Values used to determine total radioactivity PK parameters were calculated by converting the raw data generated by LSC to concentrations (ng-eq./mL) using the specific activity of administered [^{3}H]**1a** or [^{3}H]**1b**. The $AUC_{0-tlast}$ was calculated using the linear trapezoidal method, k_{el} was determined by linear regression of the log concentration versus time data during the last observable elimination phase, and half-life ($t_{1/2}$) was calculated as $0.693/k_{el}$. Both C_{max} and the time of its occurrence (T_{max}) were taken directly from the concentration vs. time data. Means and standard deviations were calculated when half or greater of the values exceeded the LLOQ for total radioactivity (2 and 10 ng-eq./mL for rats and dogs, respectively). A value of 0 was used when a measured value was <LLOQ.

Preparation of [^{3}H]1b Samples for Metabolite Profiling and Identification. At each step during the sample preparation of all biological matrices, total radioactivity levels were determined by LSC for recovery calculations. Following preparation, all samples were analyzed as described below by LC-MS/MS with radiometric detection. Pre-dose and blank samples served as controls for determining background radioactivity

and endogenous, non-drug-related ions observed within respective matrices or their extracts by LC-MS/MS.

Urine. LSC analysis of both pre- and post-lyophilization urine samples for each time point from each animal found no significant difference (i.e. ±5%) in the amount of radioactivity contained within each sample suggesting that no appreciable amount of HTO was contained within this matrix. Thus, non-lyophilized urine samples from each rat (collected from 0–48 h post-dose representing >93% of total urine radioactivity) and dog (0–24 h or 0–48 h samples, >95% of total urine radioactivity) were pooled proportional to the amount of urine in each sampling period to afford the analytical sample.

Feces. Due to minimal amounts of fecal radioactivity recovered from dogs (<3% of dose), only rat feces were profiled. Fecal homogenates (6 to 14 g) from each rat collected from 0–48 h post-dose representing >94% of total fecal radioactivity were pooled proportional to the amount of feces in each sampling period. Pooled homogenates were diluted with acetonitrile (MeCN; 2 mL/g homogenate), vortex-mixed and centrifuged (1,811 rcf for 10 min), and the resulting supernatants were isolated. If necessary, the remaining fecal pellets were extracted further with 40% H_2O in MeCN (4×6 mL) until >90% of the radioactivity from each pooled sample was recovered. The supernatants were concentrated to near dryness and reconstituted in 30% MeCN in 10 mM ammonium formate, pH 3.4 (750 μL, Solvent A) for analysis. Although fecal homogenates did not undergo lyophilization for the determination of HTO content, HTO within analytical samples was evaluated by monitoring the elution of a peak within or close to the solvent front of the radiochromatogram. In all rat fecal extracts analyzed, no radioactive peak

DMD Fast Forward. Published on June 21, 2006 as DOI: 10.1124/dmd.106.010934
This article has not been copyedited and formatted. The final version may differ from this version.

corresponding to ≥1% of the administered dose was observed within the radiochromatogram during the first 15 min post-injection.

Rat Plasma. Non-lyophilized plasma from blood samples collected at 0.5, 1, 2, 4 and 8 h post-dose were used for circulatory metabolite profiling and identification since ca. 90% of the lyophilized total radioactivity $AUC_{0–24}$ was captured by its $AUC_{0–8}$, and ca. 80% of the total non-lyophilized radioactivity $AUC_{0–8}$ was captured by its lyophilized $AUC_{0–8}$, suggesting little contribution to the non-lyophilized total radioactivity $AUC_{0–8}$ by HTO. Plasma samples were pooled within gender according to the method of Hamilton *et al.* (Hamilton et al., 1981); i.e. 17, 25, 50, 100 and 67 μL, respectively, of plasma from each time point sample were combined to afford 259 μL of pooled plasma for each gender profile. To remove dissolved proteins, the male and female pooled plasma samples were diluted with MeCN (1.04 mL), vortex-mixed for 30 min, centrifuged (2,465 rcf for 10 min) and the resulting supernatants, which contained >83% of the radioactivity from each pooled plasma sample, were isolated. Each supernatant was concentrated to near dryness at 35 °C under N_2, and reconstituted in Solvent A (150 μL) for analysis.

Dog Plasma. Non-lyophilized plasma from blood samples collected at 0.25, 0.5, 1, 2, 3, 4 and 6 h post-dose were used for circulatory metabolite profiling and identification since ca. 90% of the total radioactivity $AUC_{0–12}$ was captured by its $AUC_{0–6}$ using either non-lyophilized or lyophilized sample data, and ca. 100% of the total non-lyophilized radioactivity $AUC_{0–6}$ was captured by its lyophilized $AUC_{0–6}$, suggesting no HTO contribution to the non-lyophilized total radioactivity $AUC_{0–6}$. Plasma samples were pooled as described above such that 125, 375, 750, 1,000, 1,000, 1,500 and 1,000 μL,

DMD Fast Forward. Published on June 21, 2006 as DOI: 10.1124/dmd.106.010934
This article has not been copyedited and formatted. The final version may differ from this version.

respectively, of plasma from each time point sample per animal were combined. Thus, since 2 dogs/sex were dosed, a total of 11.5 mL of pooled plasma was obtained for each gender profile. The pooled plasma samples were diluted with MeCN (23 mL), vortex-mixed for 30 min, centrifuged (2,465 rcf for 10 min) and the resulting supernatants, which contained >94% of the radioactivity from each pooled plasma sample, were isolated. Each supernatant was concentrated to near dryness at 35 °C under N_2, and reconstituted in Solvent A (300 μL) for analysis.

Metabolite Profiling and Identification Using [^{3}H]1b Samples. Samples were analyzed by an LC-MS/MS, comprised of a PE Sciex API-3000 tandem quadrupole mass spectrometer with a Turbo Ionspray® interface (Perkin Elmer Life and Analytical Sciences, Boston, MA), two Shimadzu LC-10A HPLC pumps (Shimadzu USA, Columbia, MD) and a CTC PAL Autosampler (LEAP Technologies, Carrboro, NC), in series with a β-RAM radiometric detector (IN/US Systems, Inc., Tampa, FL) containing a liquid scintillant cell (500 μL). Analytes within sample aliquots (20–100 μL) were eluted on a Phenomenex Luna Phenyl-hexyl analytical column (5 μ, 4.6 × 250 mm) at 1 mL/min with 10 mM ammonium formate, pH 3.4 (Solvent B) and MeCN (Solvent C). The following two-step gradient was employed: 0–10 min, 2% solvent C in solvent B; 10–30 min, 2%–35% C in B; 30–32 min, 35%–90% C in B. Following the elution of **1** and its metabolites, the column was washed with 90% C in B for 3 min and then returned over 3 min to 2% C in B where it remained for 7 min prior to the next injection. For each matrix, >94% of the radioactivity injected onto the column eluted during the first 32 min of the gradient program. HPLC effluent was split 1:9 between the mass spectrometer and the radiometric flow detector; liquid scintillation cocktail flowed at 3 mL/min to the

radiometric detector. Mass spectral data were collected using positive ionization in full, precursor ion, neutral loss, product ion and multiple-reaction monitoring scanning modes. Instrument settings and potentials were adjusted to provide optimal data in each mode. Masschrom version 1.1.1 (Perkin Elmer Life and Analytical Sciences) and Winflow version 1.4 (IN/US Systems, Inc.) software were used for the acquisition and processing of mass spectral and radiochromatographic data, respectively.

Results

Excretion of Total Radioactivity in Rats and Dogs Administered [^{3}H]1a or [^{3}H]1b. Due to no readily apparent gender-related differences in overall excretory routes or mass recoveries in either species, averages (with standard deviations if applicable) of combined male and female radioactivity recovery values in rats and dogs after [^{3}H]**1b** administration are listed in Table 1; [^{3}H]**1a** pilot study mass balance values are also tabulated for comparison, and only consist of 2 rats and 1 dog. The excretion of total radioactivity derived from either [^{3}H]**1a** or [^{3}H]**1b** was rapid in both species; on average, >70% of the administered radioactivity was excreted within the first 24 h predominately renally. For [^{3}H]**1a**, only 80% mass balance was achieved in rats with urinary HTO accounting for 4% of recovered dose, while 95% mass balance was attained in dogs with no detection of HTO. For [^{3}H]**1b**, mass balance was achieved in both rats and dogs with <1% of the dose detected as HTO in cumulative excreta from either species.

Pharmacokinetics of Total Radioactivity in Rats Administered [^{3}H]1a or [^{3}H]1b. For [^{3}H]**1a**-derived data, total radioactivity plasma concentration versus time curves are plotted in Figure 2 and PK parameters are listed in Table 2. For [^{3}H]**1b**-related data, all reported PK parameters (Table 2) are an average of genders due to no readily apparent gender-related differences in systemic exposures to total radioactivity; average total radioactivity plasma concentration versus time curves for both non-lyophilized and lyophilized plasma are plotted in Figure 4. For [^{3}H]**1b**, mean total radioactivity T_{max} and C_{max} were identical for non-lyophilized and lyophilized plasma samples, while the non-lyophilized plasma $t_{1/2}$ was greater (31 vs. 24 h). Interestingly, [^{3}H]**1b** total radioactivity AUC ratios of lyophilized versus non-lyophilized plasma decreased for AUC_{0-8} (0.8),

DMD Fast Forward. Published on June 21, 2006 as DOI: 10.1124/dmd.106.010934
This article has not been copyedited and formatted. The final version may differ from this version.

$AUC_{0–24}$ (0.5) and $AUC_{0–\infty}$ (0.2), suggestive of HTO within non-lyophilized plasma from blood drawn at later time points post-dose, which rationalizes the longer non-lyophilized plasma $t_{1/2}$. If HTO was indeed present in plasma, it must have arisen from a minimal amount of drug-related material since <1% of the [^{3}H]**1b** dose detected in rat urine was attributable to HTO and overall mass recovery was high (93%).

A comparison of [^{3}H]**1a** (8 mg/kg) to [^{3}H]**1b** (5 mg/kg) non-lyophilized plasma total radioactivity PK parameters clearly shows a significant difference in total radioactivity exposure (Table 2). Although T_{max} was identical and C_{max} was dose-proportional for both radioisomers, total radioactivity AUC ratios for [^{3}H]**1a** versus [^{3}H]**1b** increased non-linearly for $AUC_{0–8}$ (4.5) and $AUC_{0–\infty}$ (28). Accordingly, non-lyophilized plasma total radioactivity half-lives for [^{3}H]**1a** and [^{3}H]**1b** were 133 and 31 h, respectively, with the former being consistent with that of 85–98 h reported previously for HTO in rats (Richmond et al., 1962; Foy, 1964; Wheeler et al., 1972). Although greater ^{3}H-exposure in rats attained by [^{3}H]**1a** relative to [^{3}H]**1b** could hypothetically be due to an isotope effect altering the metabolic profile to longer-lived and/or more slowly cleared metabolite(s), a combination of PK data indicative of substantial systemic HTO, the presence of urinary HTO, and incomplete mass balance for [^{3}H]**1a** versus [^{3}H]**1b** implicated instead HTO arising from the unique loss of tritium originally within [^{3}H]**1a**.

Pharmacokinetics of Total Radioactivity in Dogs Administered [^{3}H]1a or [^{3}H]1b. For [^{3}H]**1a**, total radioactivity plasma concentration versus time curves are plotted in Figure 1 and PK parameters are listed in Table 2. For [^{3}H]**1b**-related data, all reported PK parameters (Table 2) are an average of genders due to no readily apparent gender-related differences in systemic exposures to total radioactivity; average total radioactivity

DMD Fast Forward. Published on June 21, 2006 as DOI: 10.1124/dmd.106.010934
This article has not been copyedited and formatted. The final version may differ from this version.

plasma concentration versus time curves for both non-lyophilized and lyophilized plasma are plotted in Figure 5. For [^{3}H]**1b**, mean total radioactivity T_{max}, C_{max} and $t_{1/2}$ values were essentially identical for non-lyophilized and lyophilized plasma samples, confirming the absence of HTO in excreta. Additionally, non-lyophilized plasma C_{max} and AUC values for [^{3}H]**1a** (15 mg/kg) were 1.5-fold greater than those for [^{3}H]**1b** (10 mg/kg), consistent with linear PK for total radioactivity; identical T_{max} and similar $t_{1/2}$ were also observed. These PK data, supplemented by the absence of HTO in excreta and full mass recovery in both dog studies, confirmed the chemical and metabolic ^{3}H-stability within both [^{3}H]**1a** and [^{3}H]**1b** in dogs.

Structural Rationalization of 1 and Its Metabolites. Compound **1** had a protonated molecular ion of *m/z* 272 and an LC t_R of ca. 24.4 min. The CID product ion spectrum of *m/z* 272 contained fragment ions with *m/z* 163, 146, 118, 110 and 82 (Figure 6). Accordingly, precursor ion scanning of diagnostic fragment ions *m/z* 118 and 110 determined if metabolites of **1** were modified on its quinuclidine or furanopyridine moieties, respectively. A summary of all metabolite LC-MS/MS data is found in Table 3. The identification of a metabolite as a synthetic standard was determined by the compounds' indistinguishable CID spectra and LC t_R, as well as an increase in metabolite MS peak height upon addition of the authentic standard to the analytical sample.

Quantitative Profile of [^{3}H]1b and Its Metabolites in Rat and Dog Excreta and Plasma. In addition to **1**, six metabolites were observed in rat urine and five in rat feces (Table 4). Three metabolites were tentatively identified as pyridinyl-α-hydroxy acetic acid **M1**, dihydroxy-ethyl-pyridinol **M2** and hydroxyl-ethyl-pyridinol **M3**, while the

DMD Fast Forward. Published on June 21, 2006 as DOI: 10.1124/dmd.106.010934
This article has not been copyedited and formatted. The final version may differ from this version.

other three metabolites were **2**, **3** and **4**. In dog urine, **1**, **2** and **4** were detected. On average in rat and dog urine, 40.0% and 9.3%, respectively, of the dose was unchanged **1**.

In addition to **1**, metabolites **2**, **M3**, **3** and **4** were identified in rat plasma, while only **2** and **4** were observed in dog plasma (Table 4). On average in plasma, **1** comprised 29.7% and 10.1% of total circulatory radioactivity in rats and dogs, respectively.

DMD Fast Forward. Published on June 21, 2006 as DOI: 10.1124/dmd.106.010934
This article has not been copyedited and formatted. The final version may differ from this version.

Discussion

Due to the cited caveats for using ^{3}H-compounds in radiolabeled biotransformation studies, ^{3}H-stability within [^{3}H]**1a** was first evaluated in rat and dog pilot studies by monitoring its ^{3}H-recoveries in excreta (Table 1) and non-lyophilized plasma radioactivity PK curves (Figure 2). These studies generated contrasting results, with rat and dog total ^{3}H half-lives of 133 and 5 h, respectively. Although the extensive half-life in rats could hypothetically be attributed to long-lived circulatory metabolites, it seemed more reasonably explained by HTO, which has a reported half-life of 85–98 h in rats (Richmond et al., 1962; Foy, 1964; Wheeler et al., 1972), formed by ^{3}H-loss from [^{3}H]**1a**; this was confirmed by urinary HTO and low overall mass recovery. The short total radioactivity half-life and high mass recovery in dogs, both indicative of no HTO generation as confirmed by lyophilized urine, further suggested that ^{3}H-loss in rats was due to a species-specific difference in the metabolism of [^{3}H]**1a**. These data and the known metabolic vulnerability of furans (Dalvie et al., 2002) prompted the radiosynthesis of [^{3}H]**1b** with strategic monotritiation at a site envisaged to be both chemically and metabolically inert. Subsequent mass balance studies were conducted with [^{3}H]**1b** in both species with expected lower, yet very relevant, ^{3}H-exchange risk that was evaluated by HTO quantification within urine and plasma via lyophilization.

The metabolic and excretory pathways of **1** in rats and dogs were determined definitively using [^{3}H]**1b**, with ≥86% of administered radioactivity recovered on average in both species (Table 1). Lyophilization demonstrated in both species that HTO contributed to <1% of the dose recovered in urine. It also detected HTO in rat plasma after 8 h post-dose, but not in dog plasma over 24 h (Table 2). For rats, the insignificant

amount of HTO in urine, the predominant route of radioactivity excretion, suggested essentially complete ^{3}H-retention within [^{3}H]**1b** *in vivo*. Nonetheless, enough HTO (beyond experimental error) was present in rat plasma to show meaningful differences in radioactivity PK curves for non-lyophilized versus lyophilized samples (Figure 4); HTO formation from [^{3}H]**1b** is proposed by H/^{3}H-exchange via resonance of oxygen lone pair electrons with C_7 in pyridinol metabolites. The longer turnover half-time of HTO relative to **1** and its metabolites resulted in an increasing HTO-related contribution to total circulatory radioactivity over time. This phenomenon manifested in an extended terminal phase of the non-lyophilized total radioactivity plasma PK curve, which is conspicuously absent in that from lyophilized plasma due to the physical removal of HTO during the freeze-drying process. This observation stresses the need to lyophilize all plasma samples when conducting ^{3}H-labelled drug metabolism studies as lyophilized samples ensure the true AUC and k_{el} of non-HTO-related radioactivity.

Proposed metabolic pathways, incorporating customary furan biotransformation mechanisms (Schmid et al., 1980; Kobayashi et al., 1987; Sahali-Sahly et al., 1996), of **1** in rats and dogs are presented in Figure 7. Within both species, the two metabolically susceptible sites in **1** were its quinuclidine to afford **4** and its furanopyridine to generate all other metabolites. Definitive metabolite elucidation for **1** using [^{3}H]**1b** explained the ^{3}H-instability within [^{3}H]**1a** observed in rats, but not dogs. For [^{3}H]**1a**, the rationale for ^{3}H-loss prior to identifying its metabolites with [^{3}H]**1b** was chemical exchange within **1** and/or its metabolites (Figure 3, paths a and c) and/or metabolism-mediated exchange during the biotransformation of **1** and/or its metabolites (Figure 3, paths b and d). These

possibilities for [^{3}H]**1a** are explored below using definitive [^{3}H]**1b** results while considering the different sites of monotritiation within each radioisomer.

For the evaluation of chemically-mediated ^{3}H-exchange within [^{3}H]**1a**, hypothetical "electron-pushing" suggests its C_3 ^{3}H could exchange with solvent protons to afford non-radiolabeled **1** and HTO (Figure 3, path a). Retrospectively this is an important consideration, since it was determined with [^{3}H]**1b** that **1** accounted for 41% and 9% of the dose excreted in rats and dogs, respectively. However, although such chemical exchange could have contributed significantly to ^{3}H-loss for [^{3}H]**1a** *in vivo*, it proved minimal (if any) based on the dog pilot study with [^{3}H]**1a** which generated a total radioactivity half-life of 5 h and no HTO within excreta. Since the furanopyridine of [^{3}H]**1a** is unchanged in **4**, which comprised 11% and 63% of the excreted dose in rats and dogs, respectively, it too maintained its C_3 ^{3}H. For **2**, if it retained ^{3}H following its formation as predicted, then ^{3}H-loss should not occur as carboxylic acid α-Hs typically are not acidic enough for solvent exchange. Similarly, passive ^{3}H-exchange would not be expected within **M1**. For putative metabolites **M2** and **M3**, the extent of C_3 ^{3}H-exchange is unknown though it can be considered mechanistically (Figure 7). Based on proposed extensive intramolecular hydrogen bonding within **M2** that might prevent chemically-mediated ^{3}H-loss, ^{3}H-exchange is believed to most likely occur for **M3**. Thus, per [^{3}H]**1b** data (Table 4), 14% of administered [^{3}H]**1a** would be at risk for passive chemical exchange.

From a metabolism-mediated perspective, ^{3}H-loss within [^{3}H]**1a** would unquestionably occur upon its conversion to **3**, and conceivably occur during its transformation to **M1** via **2** and to **M2** via **M3** (Figure 7). For **3**, ^{3}H-loss is apparent due

DMD Fast Forward. Published on June 21, 2006 as DOI: 10.1124/dmd.106.010934
This article has not been copyedited and formatted. The final version may differ from this version.

to C_3 within [^{3}H]**1a** being quaternary in **3**; in studies with [^{3}H]**1b**, **3** accounted for 3.9% of the excreted dose confirming this as a ^{3}H-exchange pathway for [^{3}H]**1a** in rats. If **2** completely retained the [^{3}H]**1a** radiolabel as predicted, ^{3}H would also be expected to remain predominately within **M1** if it arose directly from **2** based on the mechanism of P450-mediated aliphatic hydroxylations (Groves and McClusky, 1976). Due to kinetic deuterium isotope effects for such biotransformations (Atkinson et al., 1994) and the inherently stronger bond strength of C-^{3}H versus C-H (Hu et al., 2003), hydroxylation of **2** to **M1** is expected to occur mainly (probably exclusively) via removal of the carboxylic acid α-H resulting in mostly (or complete) ^{3}H-retention. Since this hydroxylation may not occur entirely selectively, ^{3}H-loss might occur during formation of **M1** from **2**, but such ^{3}H-exchange concerns diminish if **M1** arises from the aldehyde tautomer of a dihydrodiol intermediate (Figure 7). For **M2** and **M3**, the projected extent of ^{3}H-loss from [^{3}H]**1a** during their formation is more difficult to assess since their structures are unconfirmed. However, if these molecules and proposed formation pathways are indeed correct, ^{3}H-loss would only predominately occur as **M3** is converted to **M2** via an epoxide pathway than by direct aliphatic hydroxylation as discussed above; **M2** and **M3** comprised 17% of [^{3}H]**1b**-derived material excreted in rats. Thus, if ^{3}H-loss occurred during the formation of all metabolites for which it is mechanistically conceivable, then, per [^{3}H]**1b** rat data (Table 4), 11% of dosed [^{3}H]**1a** would be at risk for metabolism-mediated ^{3}H-exchange.

Citing the rationale outlined above for those metabolites that may lose their radiolabel by chemical (**M3**) or metabolic (**M1**, **M2** and **3**) means, a maximum of 25% and 0% of administered [^{3}H]**1a** would be predicted to undergo ^{3}H-loss in rats and dogs, respectively.

DMD Fast Forward. Published on June 21, 2006 as DOI: 10.1124/dmd.106.010934
This article has not been copyedited and formatted. The final version may differ from this version.

In rats, although either [^{3}H]**1a** or [^{3}H]**1b** afforded ca. 70% dose recovery in urine, fecal dose recovery for [^{3}H]**1b** was 17 percentage points greater than that for [^{3}H]**1a** (Table 1), which equals the fecal [^{3}H]**1b**-related recovery comprised by **M1**, **M2**, **M3** and **3** (Table 4). Assuming that **M1** remains radiolabeled, **M2**, **M3** and **3** still comprise 13% of [^{3}H]**1b**-related fecal dose. Based on the mechanistic rationale discussed above, ^{3}H-loss from [^{3}H]**1a** upon formation of **M2**, **M3** or **3**, and the excretion of these non-radiolabeled metabolites into feces while HTO remained systemically beyond the excreta collection interval, may explain the difference in fecal (and total) dose recovery for [^{3}H]**1a** versus [^{3}H]**1b** in rats.

Strategic ^{3}H-placement within **1** to afford [^{3}H]**1b** at a site predicted to be both chemically and metabolically stable demonstrated that ^{3}H-loss in [^{3}H]**1a** was attributable to primarily species-specific metabolism-dependent instability as the majority of rat metabolites resulted from furanopyridine biotransformation. Interestingly, consistent with pilot [^{3}H]**1a** data in dogs, the identified canine metabolites using [^{3}H]**1b** confirmed no metabolism-mediated ^{3}H-exchange would be predicted for [^{3}H]**1a** since nearly complete metabolism of **1** occurred at its quinuclidine. Furthermore, the detection of only **1**, **2** and **4** in dogs administered [^{3}H]**1b** also verified that the ^{3}H-label within [^{3}H]**1a** was chemically stable in these compounds, further implicating the species-specific metabolites **M2**, **M3** and **3** (and possibly **M1**) for ^{3}H-loss from [^{3}H]**1a** in rats.

The presented studies underscore the importance of careful deliberation when considering ^{3}H-compounds for radiolabeled metabolism studies. Ironically, due to the intrinsic properties of the hydrogen atom, facile ^{3}H-exchange, which may readily afford a ^{3}H-compound synthetically, is often the culprit for compound unacceptability for

biotransformation studies. To ascertain this "exchange risk" quantitatively, all biological samples must undergo lyophilization to determine their HTO content, the amount of which determines unequivocally the suitability of the tritiation site from a biotransformation standpoint. Although ^{3}H-labeled compounds may instinctively be more cost effective and time efficient to synthesize than their ^{14}C brethren, such compounds from a metabolism perspective are only as good as the chemical and metabolic stability of their tritium atom.

DMD Fast Forward. Published on June 21, 2006 as DOI: 10.1124/dmd.106.010934
This article has not been copyedited and formatted. The final version may differ from this version.

Acknowledgments

The authors would like to acknowledge Drs. Marc B. Skaddan and Brad D. Maxwell for the synthesis and purification of [^{3}H]**1a** and [^{3}H]**1b**, respectively, and Dr. Donn G. Wishka and Ms. Karen M. Yates for the synthesis and purification of **1**, **2**, **3** and **4**.

References

Atkinson JK, Hollenberg PF, Ingold KU, Johnson CC, Le Tadic M-H, Newcomb M and Putt DA (1994) Cytochrome P450-Catalyzed Hydroxylation of Hydrocarbons: Kinetic Deuterium Isotope Effects for the Hydroxylation of an Ultrafast Radical Clock. *Biochemistry* **33:**10630-10637.

Chasseaud LF, Fry BJ and Gros PM (1974) Metabolic and Pharmacokinetic Study of Bucloxic Acid. *Arzneim-Forsch/Drug Res* **24:**1390-1397.

Dalvie D (2000) Recent Advances in the Applications of Radioisotopes in Drug Metabolism, Toxicology and Pharmacokinetics. *Curr Pharmaceut Des* **6:**1009-1028.

Dalvie DK, Kalgutkar AS, Khojasteh-Bakht SC, Obach RS and O'Donnell JP (2002) Biotransformation Reactions of Five-Membered Aromatic Heterocyclic Rings. *Chem Res Toxicol* **15:**269-299.

Ehlhardt WJ, Woodland JM, Baughman TM, Vandenbraden M, Wrighton SA, Kroin JS, Norman BH and Maple SR (1998) Liquid Chromatography/Nuclear Magnetic Resonance Spectroscopy and Liquid Chromatography/Mass Spectrometry Identification of Novel Metabolites of Multidrug Resistance Modulator LY335979 In Rat Bile and Human Liver Microsomal Incubations. *Drug Metab Dispos* **26:**42-51.

Foy JM (1964) The Biological Half-life of Tritiated Water in the Mouse, Rat, Guinea-pig and Rabbit under Tropical Conditions and the Effect of Climate and Saline Drinking on the Biological Half-life of Tritiated Water in the Rat. *J Cell Comp Physiol* **64:**279-282.

Gray A, Wilkinson DJ and Seddon H (2001) The Use of Tritium Radiolabelled Compounds In the Investigation of the DMPK Properties of New Pharmaceuticals, in: *Synthesis and Applications of Isotopically Labelled Compounds, Volume 7* (Pleiss U and Voges R eds), pp 496-499, John Wiley & Sons, Ltd., West Sussex.

Groves JT and McClusky GA (1976) Aliphatic Hydroxylation via Oxygen Rebound. Oxygen Transfer Catalyzed by Iron. *J Am Chem Soc* **98:**859-861.

Guroff G, Daly JW, Jerina DM, Renson J, Witkop B and Udenfriend S (1967) Hydroxylation-Induced Migration: The NIH Shift. *Science* **15:**1524-1530.

Hamilton RA, Garnett WR and Kline BJ (1981) Determination of Mean Valproic Acid Serum Levels by Assay of a Single Pooled Sample. *Clin Pharmacol Ther* **29:**408-413.

Hawkins DR, Weston KT, Chasseaud LF and Franklin ER (1977) Fate of Methoprene (Isopropyl (2*E*,4*E*)-11-Methoxy-3,7,11-trimethyl-2,4-dodecadienoate) in Rats. *J Agr Food Chem* **25:**398-403.

Hu Y, Dehal SS, Hynd G, Jones GB and Kupfer D (2003) CYP2D6-mediated Catalysis of Tamoxifen Aromatic Hydroxylation with an NIH Shift: Similar Hydroxylation Mechanism In Chicken, Rat and Human Liver Microsomes. *Xenobiotica* **33:**141-151.

Kim H, Prelusky D, Wang L, Hesk D, Palamanda J and Nomeir AA (2004) The Importance of Radiochemical Analysis of Biological Fluids Before and After Lyophilization From Animals Dosed with [^{3}H]-Labeled Compounds in Drug Discovery. *Am Pharmaceut Rev* **7:**44-48.

Kler RS, Sherratt HSA and Turnbull DM (1992) The Measurement of Mitochondrial β-Oxidation by Release of $^{3}H_2O$ from [9,10-^{3}H]Hexadecanoate: Application to Skeletal Muscle and the Use of Inhibitors as Models of Metabolic Disease. *Biochem Med Metab Biol* **47:**145-156.

Kobayashi T, Sugihara J and Harigaya S (1987) Mechanism of Metabolic Cleavage of a Furan Ring. *Drug Metab Dispos* **15:**877-881.

Koller-Lucae SKM, Suter MJ-F, Rentsch KM, Schott H and Schwendener RA (1999) Metabolism of the New Liposomal Anticancer Drug N^4-Octadecyl-1-β-D-Arabinofuranosylcytosine In Mice. *Drug Metab Dispos* **27:**342-350.

Larsson H and Lund J (1981) Metabolism of Femoxetine. *Acta Pharmacol et Toxicol* **48:**424-432.

Lewis CJ, Havler ME, Humphrey MJ, Lloyd-Jones JG, McCleavy MA, Muir NC and Waltham K (1988) The Pharmacokinetics and Metabolism of Idazoxan In the Rat. *Xenobiotica* **18:**519-532.

Linnet K (2004) *In vitro* microsomal metabolism of imipramine under conditions mimicking the *in vivo* steady-state situation. *Hum Psychopharmacol* **19:**31-36.

Maxwell BD, Wishka DG, Yates KM and Rogers BN (2006) Preparation of [^{3}H]PHA-543613, an Agonist of the α7 Nicotinic Acetylcholine Receptor, and Observation of a Unique 1,4-Shifted Tritiated Product. *J Label Compd Radiopharm* **submitted**.

McCarthy KE (2000) Recent Advances in the Design and Synthesis of Carbon-14 Labelled Pharmaceuticals from Small Molecule Precursors. *Curr Pharmaceut Des* **6:**1057-1083.

Prakash C, Kamel A, Gummerus J and Wilner K (1997) Metabolism and Excretion of a New Antipsychotic Drug, Ziprasidone, in Humans. *Drug Metab Dispos* **25:**863-872.

Richmond CR, Langham WH and Trujillo TT (1962) Comparative Metabolism of Tritiated Water by Mammals. *J Cell Comp Physiol* **59:**45-53.

Robertson JS (1973) Tritium Turnover Rates in Mammals, in: *Tritium Symposium* (Moghissi AA ed, pp 322-327, Messenger Graphics, Phoenix.

Rosenborg J, Larsson P, Tegner K and Hallstrom G (1999) Mass Balance and Metabolism of [^{3}H]Formoterol In Healthy Men After Combined I.V. and Oral Administration-Mimicking Inhalation. *Drug Metab Dispos* **27:**1104-1116.

Sahali-Sahly Y, Balani SK, Lin JH and Baillie TA (1996) *In Vitro* Studies on the Metabolic Activation of the Furanopyridine L-754,394, a Highly Potent and Selective Mechanism-Based Inhibitor of Cytochrome P450 3A4. *Chem Res Toxicol* **9:**1007-1012.

Saljoughian M and Williams PG (2000) Recent Developments in Tritium Incorporation for Radiotracer Studies. *Curr Pharmaceut Des* **6:**1029-1056.

Schmid J, Prox A, Reuter A, Zipp H and Koss FW (1980) The Metabolism of 8-Methoxypsoralen in Man. *Eur J Drug Metabol Pharmacokinet* **5:**81-92.

Wheeler JK, Moghissi AA, Rehnberg BF and Colvin MC (1972) Comparison Between the Biological Half-life of a Tritiated Luminous Compound with that of Tritiated Water in Rats and Cats. *Health Phys* **22:**35-38.

Wishka DG, Walker DP, Yates KM, Reitz SC, Jia S, Myers JK, Olson KL, Jacobson EJ, Wolfe ML, Groppi VE, Hanchar AJ, Thornburgh BA, Cortes-Burgos LA, Wong E, Staton BA, Raub TJ, Higdon NR, Wall TM, Hurst RS, Walters RR, Hoffman WE, Hajos M, Franklin S, Carey G, Gold LH, Cook KK, Sands SB, Zhao SX, Soglia JR, Kalgutkar AS, Arneric SP and Rogers BN (2006) Discovery of PHA-543,613, an Agonist of the α7 Nicotinic Acetylcholine Receptor, for the Treatment of Cognitive Deficits in Schizophrenia: Synthesis and SAR. *J Med Chem* **in press**.

Footnote

M.G. current address: Novartis Institutes for BioMedical Research, Department of Metabolism and Pharmacokinetics, 250 Massachusetts Ave., Cambridge, MA 02139

DMD Fast Forward. Published on June 21, 2006 as DOI: 10.1124/dmd.106.010934
This article has not been copyedited and formatted. The final version may differ from this version.

Legends for Figures

Figure 1. Chemical structures for [^{3}H]**1a** and [^{3}H]**1b**. T: ^{3}H.

Figure 2. Semi-logarithmic (top) and linear (bottom) plots of non-lyophilized plasma total radioactivity concentrations in rats (diamonds) and dogs (triangles) after oral administration of [^{3}H]**1a**.

Figure 3. Hypothetical chemical- and metabolism-mediated ^{3}H-exchange pathways for [^{3}H]**1a** *in vivo*. T^+: trition; **MX**: primary metabolite; **MY**: secondary metabolite.

Figure 4. Semi-logarithmic (top) and linear (bottom) plots of non-lyophilized (filled diamonds) and lyophilized (unfilled diamonds) plasma total radioactivity concentrations in rats after oral administration of [^{3}H]**1b**.

Figure 5. Semi-logarithmic (top) and linear (bottom) plots of mean non-lyophilized (filled triangles) and lyophilized (unfilled triangles) plasma total radioactivity concentrations in dogs after oral administration of [^{3}H]**1b**.

Figure 6. Collision-induced dissociation fragmentation pathway for protonated **1** (*m/z* 272).

Figure 7. An overview of the proposed metabolic and mechanistic pathways for **1** in rats and dogs. Bold numerical designations are for structures that were detected analytically;

DMD Fast Forward. Published on June 21, 2006 as DOI: 10.1124/dmd.106.010934
This article has not been copyedited and formatted. The final version may differ from this version.

all other structures were not detected and are solely putative metabolite intermediates. [O]: enzyme-mediated oxidation; H_2: enzyme-mediated reduction; T_a: site of ^3H within [^3H]**1a**; T_b: site of ^3H within [^3H]**1b**.

DMD Fast Forward. Published on June 21, 2006 as DOI: 10.1124/dmd.106.010934
This article has not been copyedited and formatted. The final version may differ from this version.

Tables

Table 1. Cross-species mass recoveries (% of dose) and excretory routes after oral administration of [^{3}H]**1a** or [^{3}H]**1b**

	Rat[a]				Dog[b]			
	Urine	Feces	HTO	Total[c]	Urine	Feces	HTO	Total[c]
[^{3}H]**1a**	69	6	4	80	83	10	—	95
[^{3}H]**1b**	70 ± 9	23 ± 2	—	93 ± 9	75 ± 13	2 ± 1	—	86 ± 8

—: <1% of dose.

[a]Recovery is for 0–96 h post-dose.

[b]Recovery is for 0–48 h post-dose.

[c]Total is a sum of excreta, HTO and cage debris/rinse dose recoveries.

DMD Fast Forward. Published on June 21, 2006 as DOI: 10.1124/dmd.106.010934
This article has not been copyedited and formatted. The final version may differ from this version.

Table 2. Cross-species pharmacokinetics summary for total radioactivity after oral administration of [^{3}H]**1a** or [^{3}H]**1b**

	Rat			Dog		
	[^{3}H]**1a** wet	[^{3}H]**1b** wet	[^{3}H]**1b** lyophilized	[^{3}H]**1a** wet	[^{3}H]**1b** wet	[^{3}H]**1b** lyophilized
T_{max} (h)	0.5	0.5	0.5	0.5	0.5 ± 0.0	0.5 ± 0.0
C_{max}[a]	343	382	370	947	961 ± 358	1010 ± 377
$t_{1/2}$ (h)	133	31.1	24.1	5.0	3.5 ± 2.5	2.5 ± 0.9
$AUC_{0–8}$[a]	2500	890	694	1950	2010 ± 590	2120 ± 610
$AUC_{0–12}$[a]	nd	nd	nd	nd	2130 ± 630	2230 ± 640
$AUC_{0–24}$[a]	nd	1710	788	nd	nd	nd
$AUC_{0–\infty}$[a]	62500	3560	848	2310	2250 ± 750	2310 ± 700

nd: not determined.

[a]Dose-normalized C_{max} (ng-eq.·kg·mL^{-1}·mg^{-1}) and AUC (ng-eq.·h·kg·mL^{-1}·mg^{-1}) values.

DMD Fast Forward. Published on June 21, 2006 as DOI: 10.1124/dmd.106.010934
This article has not been copyedited and formatted. The final version may differ from this version.

Table 3. Chromatographic and mass spectral data for **1** and its metabolites

Compound	LC t_R (min)	$[M+H]^+$ (*m/z*)	CID-generated Fragments[a] (*m/z*)	PC 118[b]	PC 110[c]
1	23.6	272	254, 163, 146, 118, **110**, 82	+	+
M1	16.6	322	276, 150, 127, 122, **110**, 82	–	+
M2	17.2	308	290, 272, 164, 136, 127, **110**, 82	–	+
2	19.5	306	288, 262, 180, 162, 152, 127, **110**, 82	–	+
M3	20.1	292	274, 166, 138, 127, **110**, 82	–	+
3	21.0	292	**274**, 257, 229, 148, 110, 82	–	+
4	24.3	288	164, 146, 118, **109**, 82	+	–

+: $[M+H]^+$ detected; –: $[M+H]^+$ not detected.

[a]Bold font denotes base peak *m/z* within CID spectrum.

[b]MS response for a precursor ion *m/z* 118 scan.

[c]MS response for a precursor ion *m/z* 110 scan.

DMD Fast Forward. Published on June 21, 2006 as DOI: 10.1124/dmd.106.010934
This article has not been copyedited and formatted. The final version may differ from this version.

Table 4. Cross-species comparison of excretory and circulatory metabolite profiles after oral administration of [^{3}H]**1b**

	Rat			Dog		
Recovery[a]	93.4			88.2		
	Urine	Feces	Plasma	Urine	Feces	Plasma
Dose excreted[a]	70.4	23.0	na	75.9	2.9	na
^{3}H in matrix profiled (%)	94.0	76.1	76.1	97.0	na	94.1
	Metabolite Profile[b]					
1	40.0	1.0	29.7	9.3	nd	10.1
M1	2.5	2.2	—	—	nd	—
M2	1.3	1.4	—	—	nd	—
2	5.1	1.5	11.7	1.2	nd	2.7
M3	4.5	9.3	11.7	—	nd	—
3	1.8	2.1	4.2	—	nd	—
4	11.0	—	18.8	63.1	nd	81.3

na: not applicable; nd: not determined; —: not detected.

[a]% of dose.

[b]% of dose for excretory metabolites, % of total radioactivity $AUC_{0-tlast}$ for circulatory metabolites.

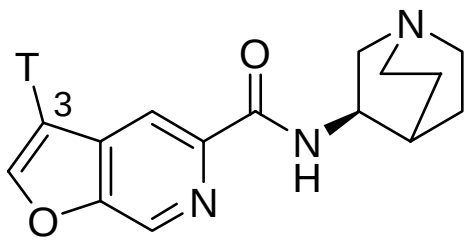

[^{3}H]**1a**

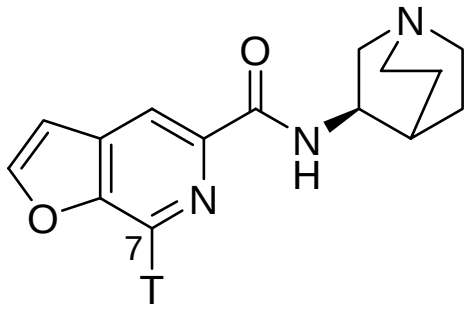

[^{3}H]**1b**

Figure 1

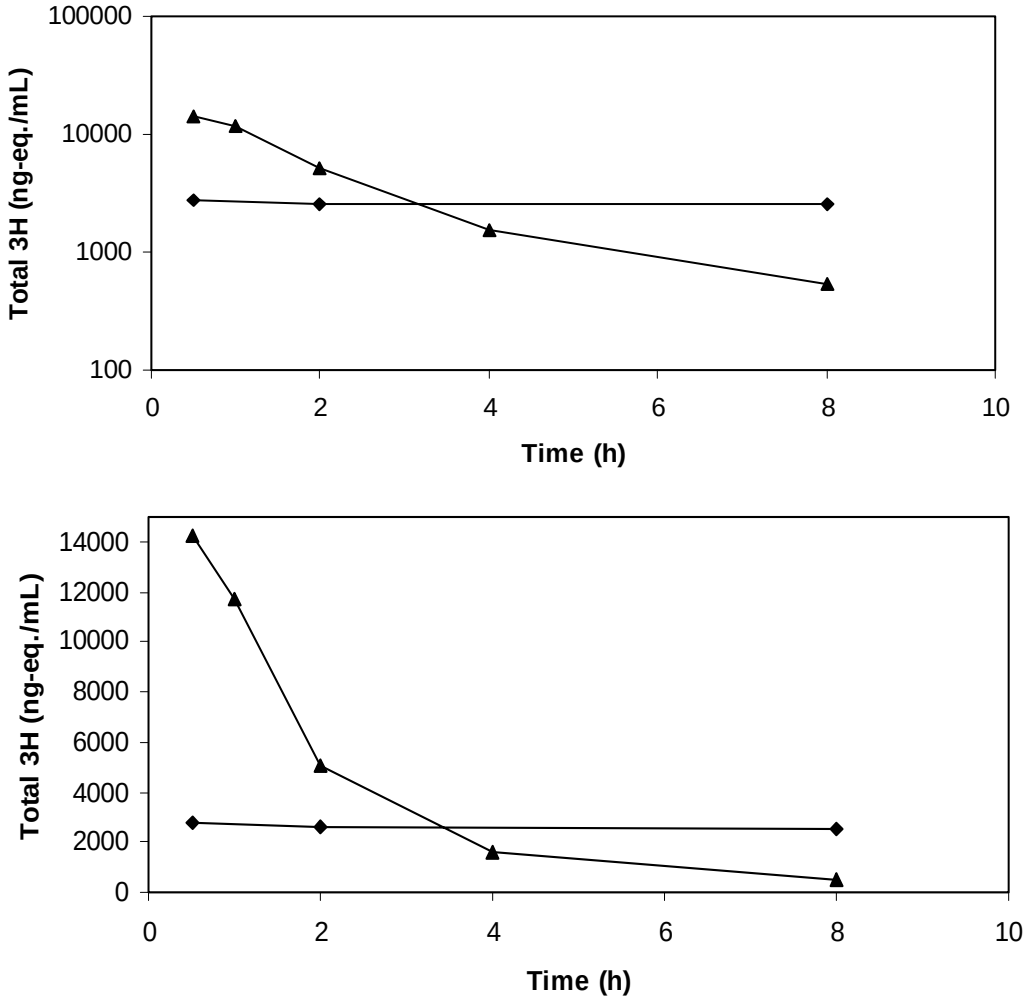

Figure 2

DMD Fast Forward. Published on June 21, 2006 as DOI: 10.1124/dmd.106.010934
This article has not been copyedited and formatted. The final version may differ from this version.

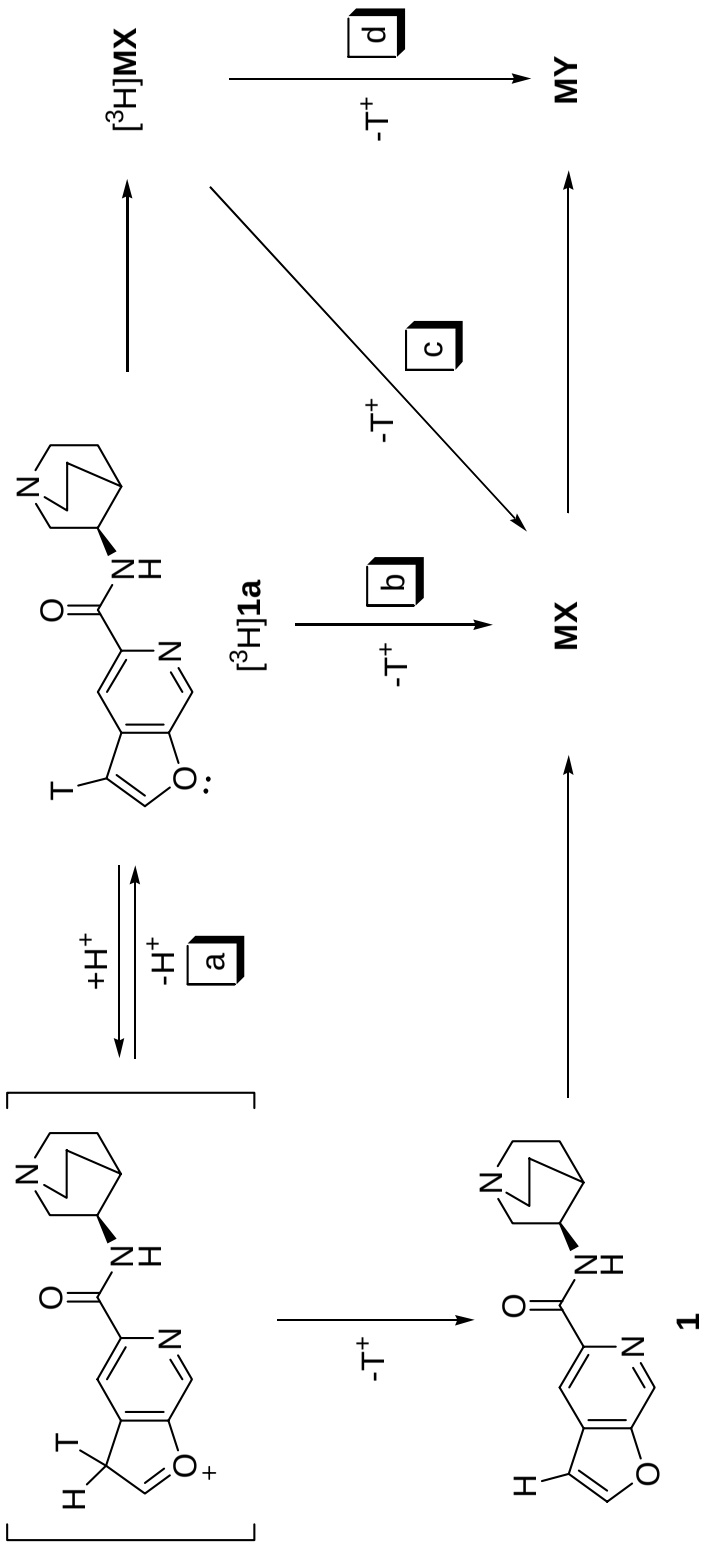

Figure 3

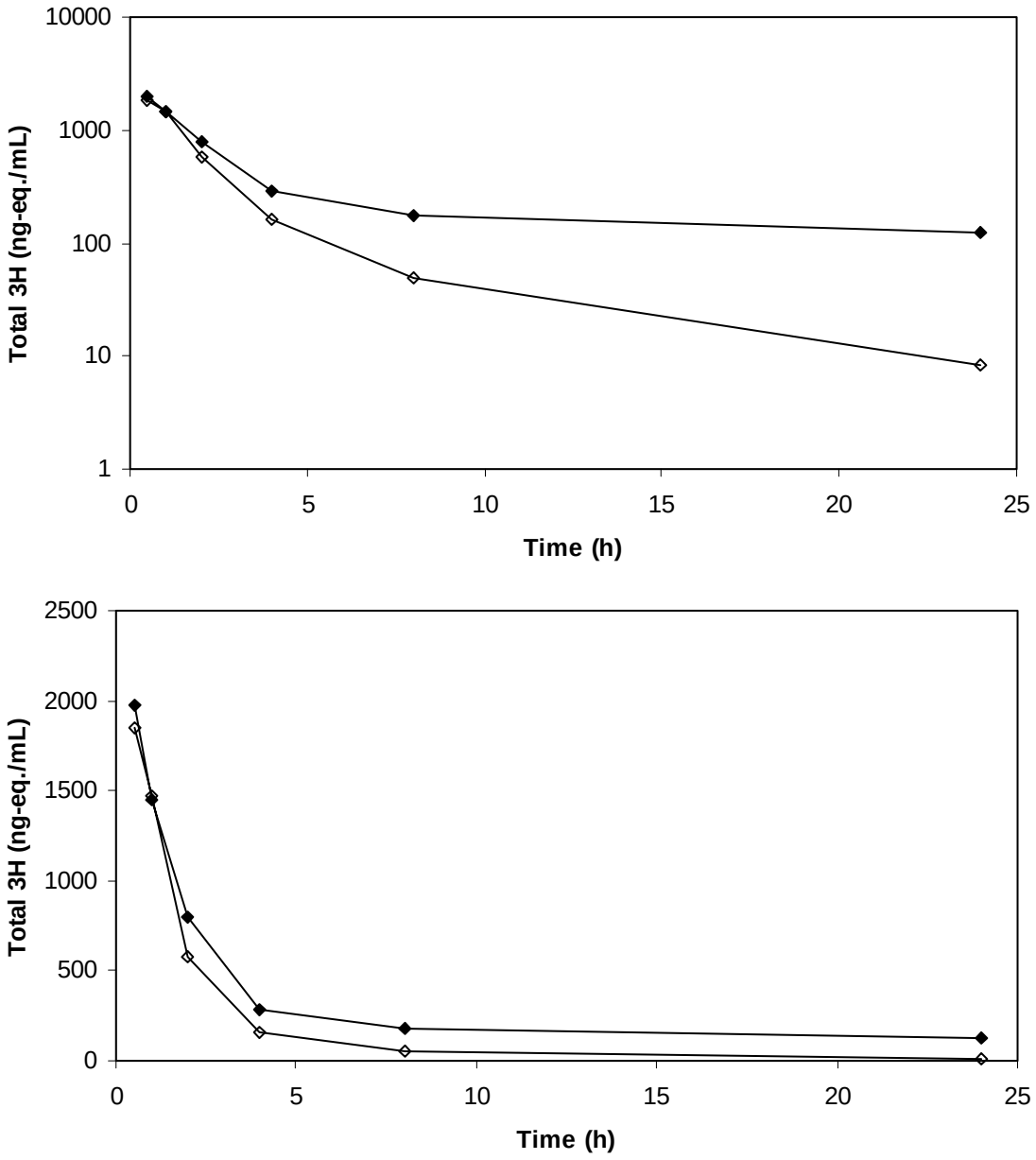

Figure 4

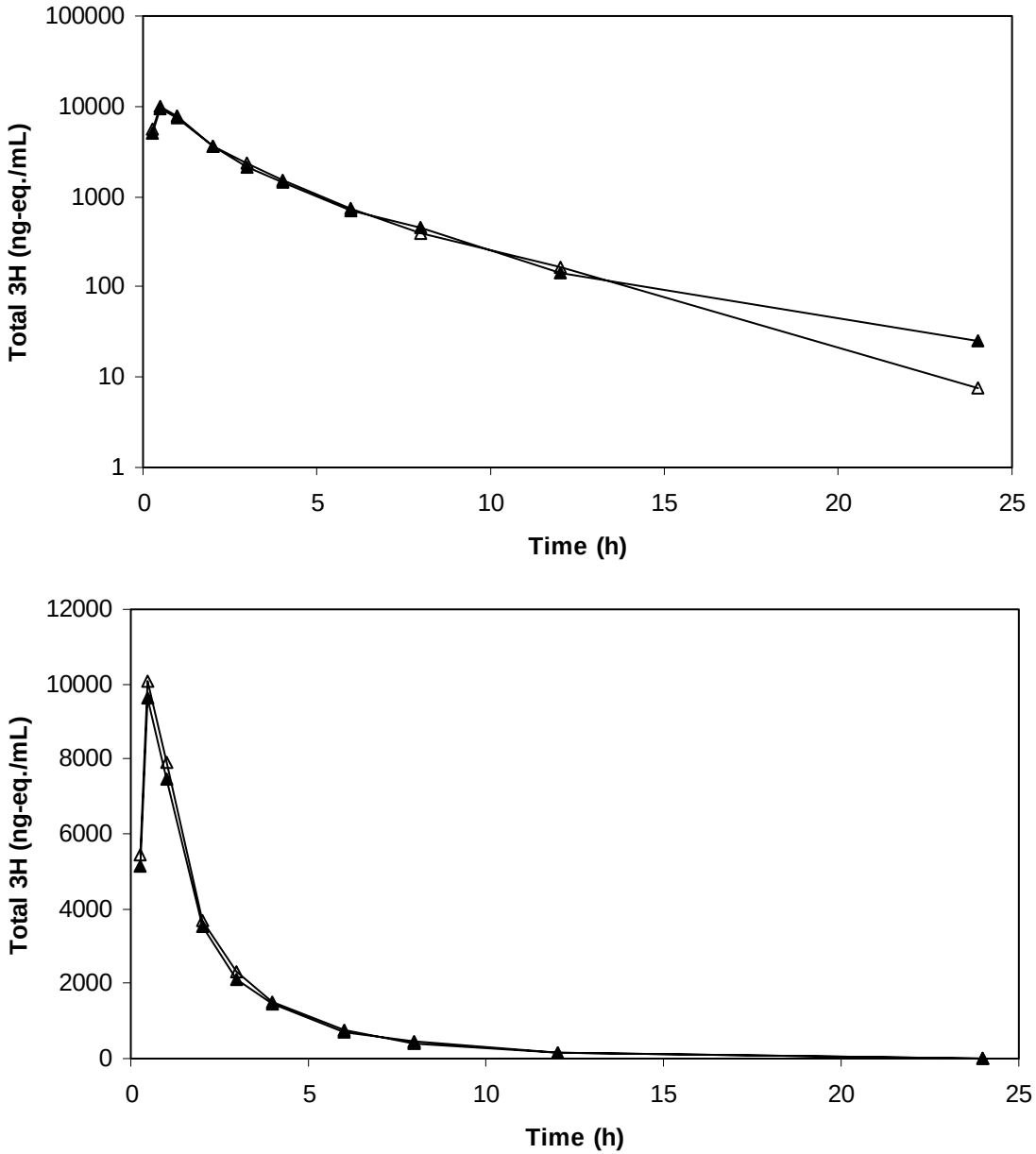

Figure 5

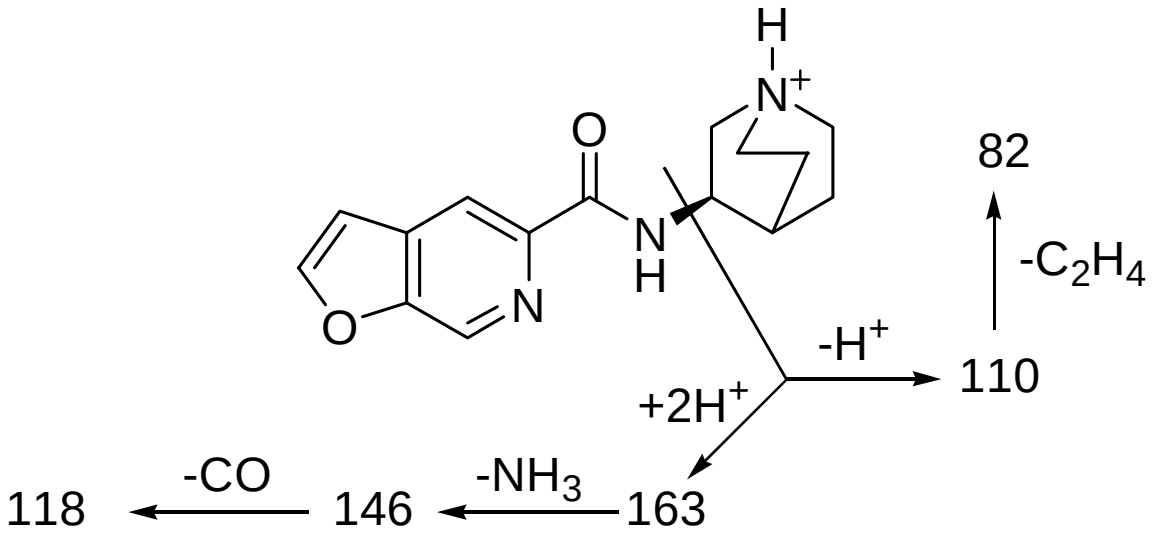

Figure 6

DMD Fast Forward. Published on June 21, 2006 as DOI: 10.1124/dmd.106.010934
This article has not been copyedited and formatted. The final version may differ from this version.

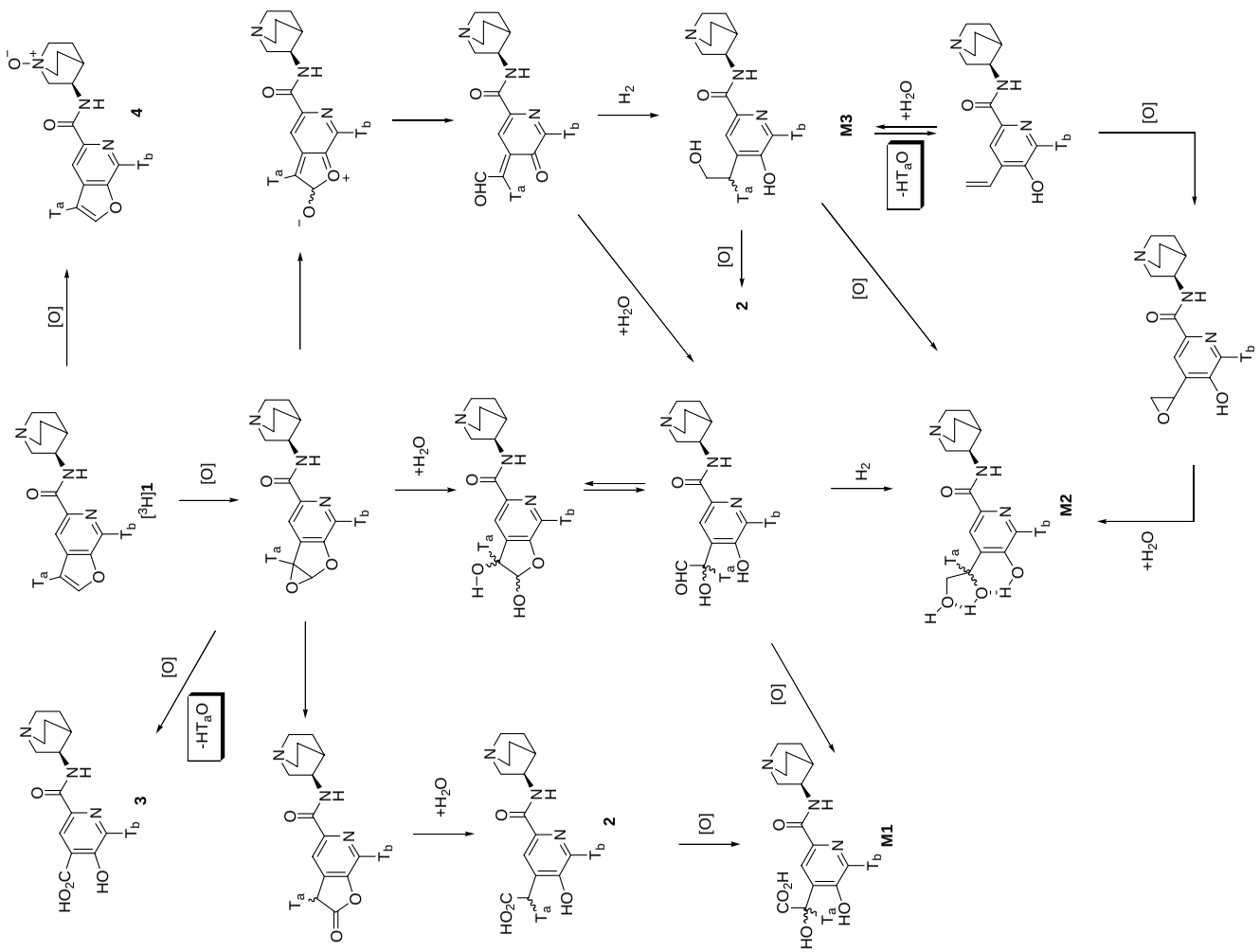

Figure 7